Anti-Interference High-Speed Modulation Decoder for Quantum Key Distribution

Hua-Xing Xu(许华醒)[1,2*], Shao-Hua Wang(王少华)[1,2], Chang-Lei Wang(王昌雷)[1,2], and Ping Zhang(张平)[1,2]

[1]*National Engineering Research Center for Public Safety Risk Perception and Control by Big Data, China Academic of Electronics and Information Technology, Beijing 100041, China*
[2]*CETC Academy of Electronics and Information Technology Group Co., Ltd., Beijing 100041, China*

(Received 30 September 2024; accepted manuscript online 25 December 2024)

Quantum key distribution is increasingly transitioning toward network applications, necessitating advancements in system performance, including photonic integration for compact designs, enhanced stability against environmental disturbances, higher key rates, and improved efficiency. In this letter, we propose an orthogonal polarization exchange reflector Michelson interferometer model to address quantum channel disturbances caused by environmental factors. Based on this model, we designed a Sagnac reflector-Michelson interferometer decoder and verified its performance through an interference system. The interference fringe visibility exceeded 98% across all four coding phases at 625 MHz. These results indicate that the decoder effectively mitigates environmental interference while supporting high-speed modulation frequencies. In addition, the proposed anti-interference decoder, which does not rely on magneto-optical devices, is well-suited for photonic integration, aligning with the development trajectory for next-generation quantum communication devices.

DOI: 10.1088/0256-307X/42/1/010303 CSTR: 32039.14.0256-307X.42.1.010303

Quantum key distribution (QKD) allows two authenticated, distant participants, Alice and Bob, to share a long random string, commonly referred to as cryptographic keys. These keys facilitate perfectly secure communications via a one-time pad. QKD has been proven to be unconditionally secure,[1–5] meaning that a QKD system based on the one-time pad algorithm can withstand eavesdroppers with unlimited abilities. The practical security of QKD has also been extensively studied. For example, the decoy state method,[6–8] which mitigates a photon-number-splitting (PNS) attack aimed at a weak coherent source, has become standard in QKD systems. Additionally, measurement device-independent (MDI) QKD has been developed to eliminate detector side-channel attacks.[9]

Over the past four decades, significant advancements have been achieved in QKD experiments utilizing different photon degrees of freedom, such as time-bin phase-based QKD[10–13] and polarization-based QKD.[14,15] These methods have been demonstrated over diverse channels, including fiber,[16–20] free space,[21–23] and other channels.[24–27] Furthermore, quantum communication networks have been studied globally.[28–35] Satellite-based quantum communication has proven capable of enabling secure global communication,[28] and long-distance integrated space-to-ground quantum communication networks[36] have been successfully constructed. To apply the increasingly mature QKD technology to standard communication networks, it is important to develop stable, efficient, cost-effective, and miniaturized QKD systems.

Time-bin phase-encoding QKD systems mainly rely on asymmetric Mach-Zehnder interferometers (AMZI),[37] which are particularly effective in situations such as when deployed along roads or bridges using overhead or tube optical cables. However, these systems are often susceptible to polarization-induced fading in transmission fibers. To address this challenge, Muller *et al.* proposed the "plug and play" bidirectional QKD system, which compensates for both polarization disturbances and phase drifts in the channel.[38] This system has been incorporated into QKD products by ID Quantique, Inc., a well-known Swiss quantum company. However, in 2006, Gisin *et al.* identified the vulnerability of "plug and play" systems to Trojan-horse attacks.[39] Subsequently, Mo *et al.* proposed the Faraday-Michelson (FM) unidirectional QKD system,[40] which has been applied in the phase-encoding QKD products by Anhui Asky Quantum Technology Co., Ltd. and incorporated into the latest time-bin phase QKD scheme patented by the University of Science and Technology of China.[41] To improve key rates of QKD systems while maintaining the stability of QKD systems to environmental variations, a gigahertz QKD scheme based on the Faraday-Sagnac-Michelson interferometer (FSMI) was proposed in Ref. [12], which increases key generation rates by decreasing insertion losses and increasing phase modulation rates. Integrated codecs utilizing Faraday mirrors have also been studied, with the mirrors acting as exterior devices.[42] Presently, effective and widely used solutions in QKD are mainly based on "plug and play" and FM schemes or their

*Corresponding author. Email: xuhuaxing@cetc.com.cn
© 2025 Chinese Physical Society and IOP Publishing Ltd. All rights, including for text and data mining, AI training, and similar technologies, are reserved.

variants, which leverage the Faraday magneto-optic effect. However, these magneto-optic-based schemes face significant challenges in achieving photonic integration, a critical trend in QKD technology.

In this study, we propose an orthogonal-polarization-exchange reflector Michelson interferometer (OPERMI) model to eliminate polarization disturbances caused by quantum channels. Based on this model, we design a Sagnac reflector-Michelson interferometer (SRMI) as a phase decoder for high-speed, efficient, and stable QKD systems and other quantum communication applications. A theoretical analysis demonstrates how the OPERMI and SRMI decoders automatically and efficiently eliminate polarization disturbances. Additionally, we constructed an interference fringe visibility system incorporating an SRMI decoder for experimental validation. The experimental results reveal that the system supports gigahertz (GHz) modulation frequency and is impervious to environmental disturbances. Compared to schemes using Faraday magneto-optic devices, our proposed scheme facilitates the photonic integration chips of QKD transceivers and receivers and can operate effectively in magnetic environments due to the absence of magneto-optic devices.

Model of Orthogonal-Polarization-Exchange Reflector Michelson Interferometer. In this section, we present a general model based on a Michelson interferometer from our previous study,[43] referred to as the quarter-wave plate reflector Michelson interferometer (QMI) scheme, to realize a stable phase-encoding QKD system.

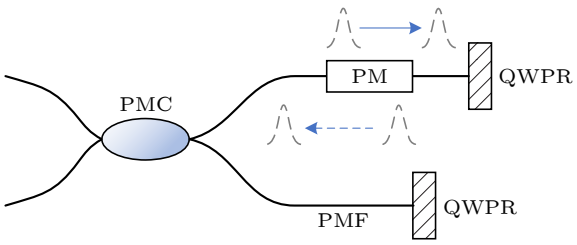

Fig. 1. Schematic of QMI. The asymmetric Michelson interferometer consists of a PMC, two unbalanced arms, a PM in the upper arm, and QWPRs.

According to Ref. [43], a QMI comprises a polarization-maintaining coupler (PMC), two unbalanced arms consisting of polarization-maintaining fibers (PMFs), and two quarter-wave plate reflectors (QWPRs), as shown in Fig. 1. Moreover, a phase modulator (PM) is placed in one of the arms. In the QMI, the arbitrarily polarized input light can be considered as two orthogonal polarization parts transferred along the slow and fast axes of the PMF arms. Upon reflection by the QWPRs, the forward-propagating light along the slow axis of the PMF arms is converted into backward light along the fast axis, and vice versa. Due to identical phase accumulation during round-trip transmission, only two orthogonal polarization states are exchanged between the input and output light. Consequently, the output polarization state becomes independent of the two arms, enabling the QMI to eliminate polarization-induced signal fading within the interferometer. This design also automatically compensates for quantum channel disturbances. The QMI scheme serves as an implementation of the OPERMI model. In QKD systems, OPERMI can automatically address channel polarization disturbances. As shown in Fig. 2, OPERMI consists of a coupler, two unbalanced arms, and two reflectors. The OPERMI model incorporates two key features:

- The two arms of the interferometer maintain two orthogonal polarizations during transmission.
- The reflector exchanges two orthogonal polarizations upon reflection.

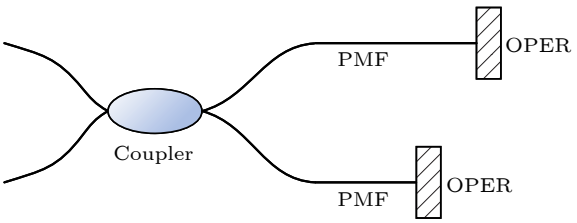

Fig. 2. Model of OPERMI. The system includes a coupler, two unbalanced arms, and two OPERs.

The function of the orthogonal-polarization-exchange reflectors (OPERs) is to exchange and reflect two orthogonal polarizations. Specifically, the state $|\Psi\rangle = a|H\rangle + b|V\rangle$ is transformed into $|\Psi'\rangle = b|H\rangle + a|V\rangle$. Since the two arms of the interferometer maintain the two orthogonal polarizations, the operator U of the OPER is defined as:

$$\begin{bmatrix} b \\ a \end{bmatrix} = U \begin{bmatrix} a \\ b \end{bmatrix},$$
$$U = \begin{bmatrix} 0 & 1 \\ 1 & 0 \end{bmatrix} = \sigma_2. \tag{1}$$

To further elucidate this stability, consider the transformation operations. When the arms of the OPERMI are constructed using PMFs, which maintain the two orthogonal polarizations during transmission, a beam of light passing through the long arm of the OPERMI and is reflected by the OPER undergoes the operation L :

$$\begin{aligned} L &= \overleftarrow{l} \cdot U \cdot \overrightarrow{l} \\ &= \begin{bmatrix} \exp\left(\frac{i\delta}{2}\right) & 0 \\ 0 & \exp\left(-\frac{i\delta}{2}\right) \end{bmatrix} \begin{bmatrix} 0 & 1 \\ 1 & 0 \end{bmatrix} \\ &\quad \cdot \begin{bmatrix} \exp\left(\frac{i\delta}{2}\right) & 0 \\ 0 & \exp\left(-\frac{i\delta}{2}\right) \end{bmatrix} \\ &= \begin{bmatrix} 0 & 1 \\ 1 & 0 \end{bmatrix} = \sigma_2, \end{aligned} \tag{2}$$

where l is the operator of the PMF long arm, $\leftarrow$ and $\rightarrow$ indicate the backward and forward propagation, respectively, and δ is the birefringence strength of the PMF long arm. A similar conclusion applies to the short-arm operator S. There is $L^\dagger L = I$, which satisfies the stable condition of the phase encoding QKD system according to Ref. [44].

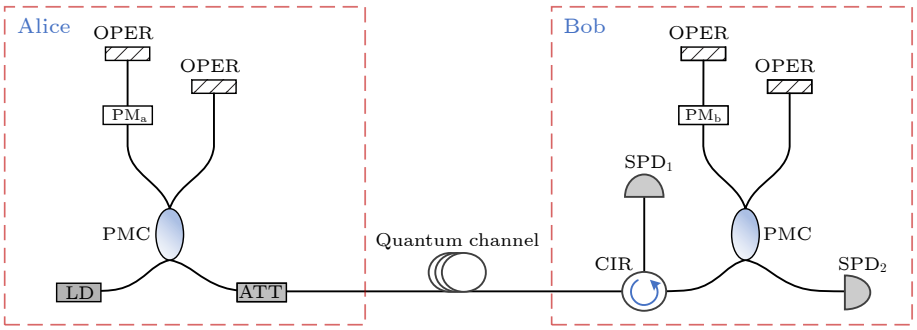

Fig. 3. Schematic of phase encoding QKD system with two OPERMIs. LD: laser diode; ATT: attenuator; CIR: optical circulator; SPDs: single-photon detectors; $\mathrm{PM_a}$ and $\mathrm{PM_b}$: phase modulators at Alice's and Bob's side, respectively.

For a QKD system with two OPERMIs serving as the encoder and decoder, as shown in Fig. 3, the transformation matrices for the two interference paths are given by

$$\begin{aligned} T_1 &= [\exp(i\varphi_{s_\mathrm{b}}) \cdot \overleftarrow{s_\mathrm{b}} \cdot U \cdot \overrightarrow{s_\mathrm{b}}] \cdot [\exp(i\varphi_c) \cdot QC] \\ &\quad \cdot [\exp(i\varphi_{l_\mathrm{a}} + i\varphi_\mathrm{a}) \cdot \overleftarrow{\mathrm{PM_a}} \cdot \overleftarrow{l_\mathrm{a}} \cdot U \cdot \overrightarrow{l_\mathrm{a}} \cdot \overrightarrow{\mathrm{PM_a}}] \\ &= \exp[i(\varphi_{s_\mathrm{b}} + \varphi_c + \varphi_{l_\mathrm{a}} + \varphi_\mathrm{a})] \cdot \sigma_2 \cdot QC \cdot \sigma_2, \\ T_2 &= [\exp(i\varphi_{l_\mathrm{b}} + i\varphi_\mathrm{b}) \cdot \overleftarrow{\mathrm{PM_b}} \cdot \overleftarrow{l_\mathrm{b}} \cdot U \cdot \overrightarrow{l_\mathrm{b}} \cdot \overrightarrow{\mathrm{PM_b}}] \\ &\quad \cdot [\exp(i\varphi_c) \cdot QC] \cdot [\exp(i\varphi_{s_\mathrm{a}}) \cdot \overleftarrow{s_\mathrm{a}} \cdot U \cdot \overrightarrow{s_\mathrm{a}}] \\ &= \exp\left[i(\varphi_{s_\mathrm{a}} + \varphi_c + \varphi_{l_\mathrm{b}} + \varphi_\mathrm{b})\right] \cdot \sigma_2 \cdot QC \cdot \sigma_2, \end{aligned} \tag{3}$$

where s_a, s_b, l_a and l_b represent the short and long arms of the interferometer, φ_{l_a}, φ_{l_b}, φ_{s_a} and φ_{s_b} are the sum of phases of the fast and slow axes of the long and short arms of the interferometers at Alice's and Bob's sides, respectively. QC represents the quantum channel, φ_c is the propagation phases of the quantum channel, φ_a and φ_b are the modulated phases of the encoder and decoder. Subscripts a and b represent Alice and Bob, respectively. Assuming the input Jones vector of the OPERMI on Alice's side is E_in, the output from Bob's interferometer is

$$\begin{aligned} E_\mathrm{out} = \frac{1}{4}\{&\exp[i(\varphi_{s_\mathrm{b}} + \varphi_c + \varphi_{l_\mathrm{a}} + \varphi_\mathrm{a})] \\ &+ \exp[i(\varphi_{s_\mathrm{a}} + \varphi_c + \varphi_{l_\mathrm{b}} + \varphi_\mathrm{b})]\} \\ &\cdot \sigma_2 \cdot QC \cdot \sigma_2 \cdot E_\mathrm{in}, \end{aligned} \tag{4}$$

The interference output power is expressed as

$$\begin{aligned} P_\mathrm{out} &= E_\mathrm{out}^\dagger \cdot E_\mathrm{out} \\ &= \frac{1}{8}[1 + \cos(\Delta\varphi_\mathrm{a} + \Delta\varphi_\mathrm{b} + \Delta\varphi_\mathrm{ab})]P_\mathrm{in}, \end{aligned} \tag{5}$$

where $\Delta\varphi_\mathrm{a} = \varphi_{l_\mathrm{a}} - \varphi_{s_\mathrm{a}}$, $\Delta\varphi_\mathrm{b} = \varphi_{l_\mathrm{b}} - \varphi_{s_\mathrm{b}}$, and $\Delta\varphi_\mathrm{ab} = \varphi_\mathrm{a} - \varphi_\mathrm{b}$. This result demonstrates that the interference output P_out is independent of polarization perturbations throughout the QKD system. Hence, the OPERMI model ensures the QKD system is unaffected by polarization disturbances caused by the quantum channel.

Sagnac Configuration-Based Orthogonal-Polarization-Exchange Reflector Michelson Interferometer Scheme. We propose a high-speed, efficient phase decoder scheme for QKD based on the OPERMI model, referred to as the SRMI. As shown in Fig. 4, the SRMI consists of a PMC, two PMF arms, two Sagnac configuration reflectors, and a PM located in one of the two reflectors. The Sagnac configuration reflector includes a PBS and a PMF with a 90° twist between its two ends. The two output ports of the PBS are connected by a 90° twisted PMF, with both ports coupled to the slow (or fast) axis of the PMF. The PM is located in the middle of the Sagnac configuration within one arm of the SRMI. Thus, when an optical pulse enters the PBS and splits into two orthogonal parts, both parts are modulated simultaneously by the PM.

The Sagnac configuration reflector has the same function as the QWPR: converting horizontal polarization to vertical polarization, and vice versa. As shown in Fig. 5, the input port of the PBS is denoted as Port A and the output ports are denoted as Port B and Port C, respectively. Assume both Port B and Port C are coupled to the slow axis of the twisted PMF (denoted as *F-s* axis). When an arbitrarily polarized pulse enters the PBS, it splits into two parts. One component, the horizontally polarized pulse (H), aligns with the *F-s* axis and exits through Port C, propagating counterclockwise (CCW). The other component, the vertically polarized pulse (V), also aligns with the *F-s* axis and exits through Port B, propagating clockwise (CW). For example, starting with horizontal polarization at Port C, the direction of H is in line with the *F-s* axis. Along the twist of the PMF, pulse H is converted to V at Port B, as shown in Fig. 5. Similarly, along the CW direction, pulse V from Port B is turned to H at Port C. Due to identical phase accumulation in both CW and CCW paths, only polarization exchange occurs after transmitting the Sagnac configuration. Thus, the Sagnac configuration reflector effectively eliminates polarization-induced fading caused by quantum channels, analogous to the QWPR does.

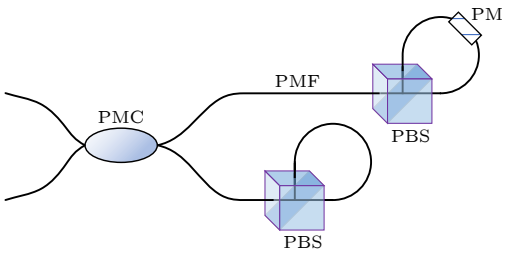

Fig. 4. Schematic of the SRMI. It contains a PMC, two unbalanced arms, two Sagnac configuration reflectors, and a PM in one reflector.

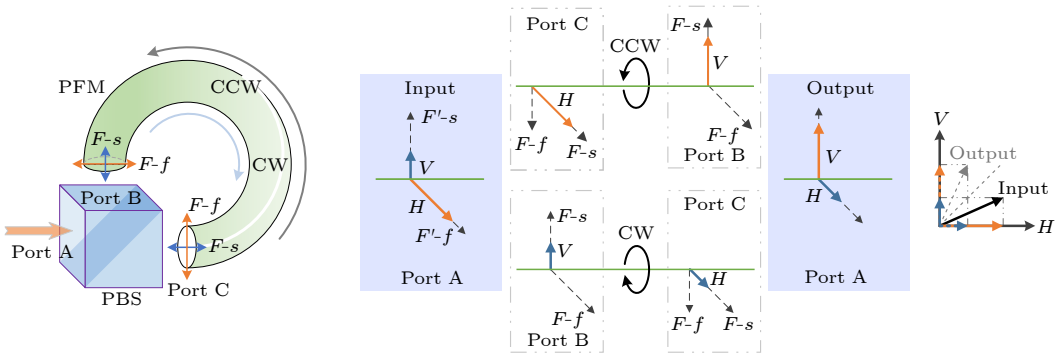

Fig. 5. Schematic of the Sagnac configuration.

The SRMI scheme enables a higher decoding rate than the QMI scheme. When a pulse enters the modulation arm, it splits into two parts by the PBS: H, which travels along the twisted PMF from Port C to Port B and V, which travels from Port B to Port C. Both PBS output ports couple to the slow (for example) axis of the PMF, allowing the PM to modulate the orthogonal polarization parts with the same phase φ. The SRMI scheme supports the use of either birefringent PMs or single-polarization PMs. In addition, the modulation voltage in the SRMI scheme only needs to remain constant over the pulse width, as the orthogonal polarization parts arrive at the PM simultaneously. Thus, the general DAC technology can provide a stable modulation voltage for a gigahertz SRMI scheme. Since the modulated pulse passes through the PM only once, the insertion loss is decreased, making the SRMI scheme more efficient than QMI and FMI schemes.

Experimental Verification. To demonstrate this theory, an interference fringe visibility test platform was constructed to evaluate the performance of the SRMI scheme, as shown in Fig. 6. In the setup, the transmitter Alice encodes key information into quantum states $\{0, \pi/2, \pi, 3\pi/2\}$, and sends quantum pulses to the receiver Bob. Alice and Bob utilize two SRMIs as the encoder and decoder, respectively. The stability of the system validates the effectiveness of the SRMI. A variable optical attenuator (ATT) on Alice's side was used to attenuate the transmitted light to the single-photon level. To simulate polarization disturbances in the quantum channel, a polarization scrambler module (PSM-002, General Photonics Corporation) working at a 10 kHz scrambling rate was incorporated. The loss from the input port to the output port for the encoder was measured to be 2.70 dB, while the losses from the input port to the output ports 1 and 2 of the decoder were 2.92 dB and 3.45 dB, respectively.

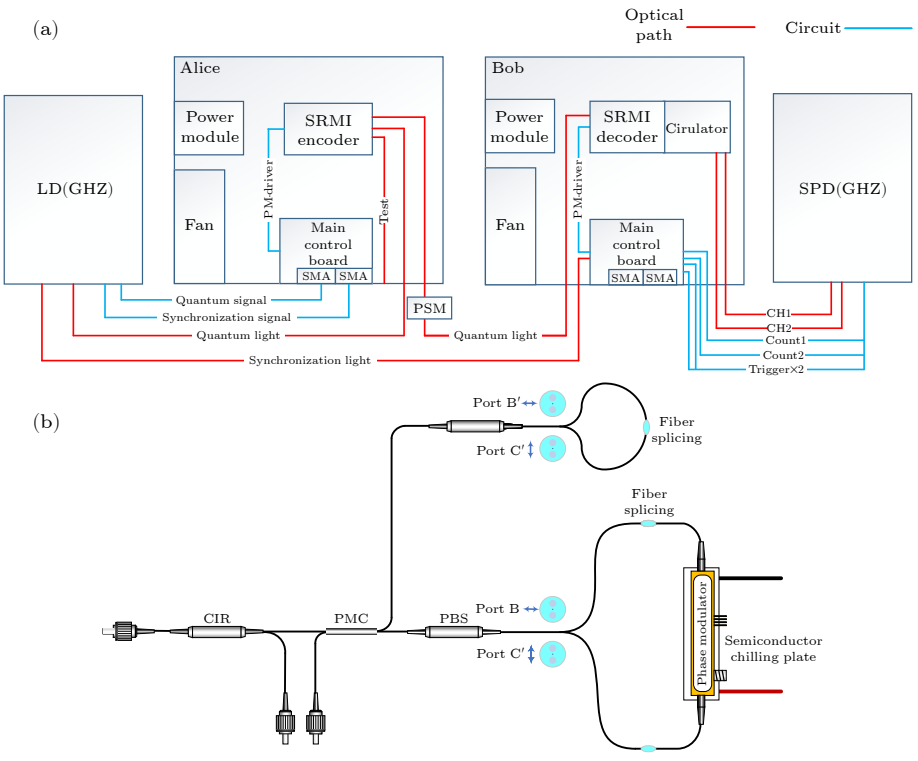

Fig. 6. (a) Schematic of the interference fringe visibility test system. (b) Structure of the Sagnac-reflector Michelson interferometer decoder.

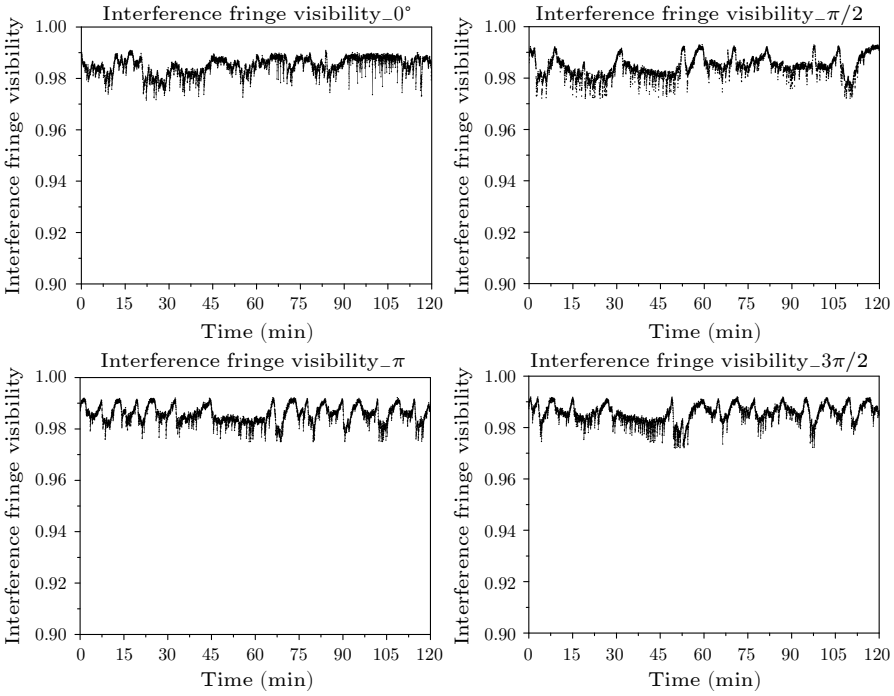

Fig. 7. Average interference fringe visibility for (a) 0, (b) $\pi/2$, (c) π, and (d) $3\pi/2$ states over 50.4 km during a 2-h period.

During the experiment, photons were generated by an attenuated distributed-feedback pulsed laser diode operating at a wavelength of 1550.12 nm, with a pulse width of 50 ps and a repetition rate of 0.625 GHz. Two high-speed single-photon detectors, also operating at 0.625 GHz, were used on Bob's side.

Based on the described setup, the interference fringe visibility for the four quantum states was measured to examine the system performance. As shown in Fig. 7, the average fringe visibilities for the states 0, $\pi/2$, π, and $3\pi/2$ were 98.16%, 98.21%, 98.50%, and 99.2%, respectively, over a coiling fiber of 50.4 km during a 2-h measurement period.

Conclusion. In this study, we proposed an OPERMI model for QKD systems, which eliminates polarization-induced fading caused by quantum channels. Based on this model, we proposed the SRMI phase decoder scheme, offering high efficiency, high-speed modulation, and robust resistance to environmental disturbances. To validate the proposed approach, an SRMI phase-decoder-based interference fringe visibility system was constructed. Experimental results revealed that the system supports high modulation frequencies and is unaffected by environmental disturbances. Notably, all components in the SRMI decoder are commercially available off-the-shelf optical components, ensuring ease of fabrication. Furthermore, the SRMI decoder does not rely on magneto-optic components, making it well-suited for photonic integration and applications in magnetic environments. This study represents a significant step toward the practical applications and miniaturization of quantum communication devices.

Acknowledgements. This work was supported by the National Natural Science Foundation of China under Grant No. 62001440.

References

[1] Mayers D 2001 *J. ACM* **48** 351
[2] Lo H K and Chau H F 1999 *Science* **283** 2050
[3] Shor P W and Preskill J 2000 *Phys. Rev. Lett.* **85** 441
[4] Renner R 2008 *Int. J. Quantum Inform.* **06** 1
[5] Ben-Or M, Horodecki M, Leung D W, Mayers D, and Oppenheim J 2005 *The Universal Composable Security of Quantum Key Distribution Theory of Cryptography* (Berlin, Heidelberg: Springer) p. 386
[6] Hwang W Y 2003 *Phys. Rev. Lett.* **91** 057901
[7] Wang X B 2005 *Phys. Rev. Lett.* **94** 230503
[8] Lo H K, Ma X, and Chen K 2005 *Phys. Rev. Lett.* **94** 230504
[9] Lo H K, Curty M, and Qi B 2012 *Phys. Rev. Lett.* **108** 130503
[10] Boaron A, Boso G, Rusca D, Vulliez C, Autebert C, Caloz M, Perrenoud M, Gras G, Bussières F, Li M J, Nolan D, Martin A, and Zbinden H 2018 *Phys. Rev. Lett.* **121** 190502
[11] Islam N T, Lim C C W, Cahall C, Kim J, and Gauthier D J 2017 *Sci. Adv.* **3** 1701491
[12] Wang S, Chen W, Yin Z Q, He D Y, Hui C, Hao P L, Fan-Yuan G J, Wang C, Zhang L J, Kuang J, Liu S F, Zhou Z, Wang Y G, Guo G C, and Han Z F 2018 *Opt. Lett. OL* **43** 2030
[13] Yuan Z, Plews A, Takahashi R, Doi K, Tam W, Sharpe A W, Dixon A R, Lavelle E, Dynes J F, Murakami A, Kujiraoka M, Lucamarini M, Tanizawa Y, Sato H, and Shields A J 2018 *Journal of Lightwave Technology* **36** 3427
[14] Agnesi C, Avesani M, Calderaro L, Stanco A, Foletto G, Zahidy M, Scriminich A, Vedovato F, Vallone G, and Villoresi P 2020 *Optica* **7** 284
[15] Grünenfelder F, Boaron A, Rusca D, Martin A, and Zbinden H 2018 *Appl. Phys. Lett.* **112** 051108
[16] Chen J P, Zhang C, Liu Y, Jiang C, Zhang W, Hu X L, Guan J Y, Yu Z W, Xu H, Lin J, Li M J, Chen H, Li H, You L, Wang Z, Wang X B, Zhang Q, and Pan J W 2020 *Phys. Rev. Lett.* **124** 070501

[17] Minder M, Pittaluga M, Roberts G L, Lucamarini M, Dynes J F, Yuan Z L, and Shields A J 2019 *Nat. Photonics* **13** 334

[18] Wang S, Yin Z Q, He D Y, Chen W, Wang R Q, Ye P, Zhou Y, Fan-Yuan G J, Wang F X, Chen W, Zhu Y G, Morozov P V, Divochiy A V, Zhou Z, Guo G C, and Han Z F 2022 *Nat. Photon.* **16** 154

[19] Zhong X, Hu J, Curty M, Qian L, and Lo H- 2019 *Phys. Rev. Lett.* **123** 100506

[20] Zhong X Q, Hu J Y, Curty M, Qian L, and Lo H K 2021 *Phys. Rev. Appl.* **15** 064016

[21] Bedington R, Arrazola J M, and Ling A 2017 *npj Quantum Inf.* **3** 30

[22] Liao S K, Cai W Q, Liu W Y, Zhang L, Li Y, Ren J G, Yin J, Shen Q, Cao Y, Li Z P, Li F Z, Chen X W, Sun L H, Jia J J, Wu J C, Jiang X J, Wang J F, Huang Y M, Wang Q, Zhou Y L, Deng L, Xi T, Ma L, Hu T, Zhang Q, Chen Y A, Liu N L, Wang X B, Zhu Z C, Lu C Y, Shu R, Peng C Z, Wang J Y, and Pan J W 2017 *Nature* **549** 43

[23] Vallone G, Bacco D, Dequal D, Gaiarin S, Luceri V, Bianco G, and Villoresi P 2015 *Phys. Rev. Lett.* **115** 040502

[24] Feng Z, Li S, and Xu Z 2021 *Opt. Express* **29** 8725

[25] Hu C Q, Yan Z Q, Gao J, Jiao Z Q, Li Z M, Shen W G, Chen Y, Ren R J, Qiao L F, Yang A L, Tang H, and Jin X M 2019 *Photon. Res. PRJ* **7** A40

[26] Wang S, Chen W, Yin Z Q, Li H W, He D Y, Li Y H, Zhou Z, Song X T, Li F Y, Wang D, Chen H, Han Y G, Huang J Z, Guo J F, Hao P L, Li M, Zhang C M, Liu D, Liang W Y, Miao C H, Wu P, Guo G C, and Han Z F 2014 *Opt. Express* **22** 21739

[27] Tang B Y, Liu B, Zhai Y P, Wu C Q, and Yu W R 2019 *Sci Rep* **9** 15733

[28] Liao S K, Cai W Q, Handsteiner J, Liu B, Yin J, Zhang L, Rauch D, Fink M, Ren J G, Liu W Y, Li Y, Shen Q, Cao Y, Li F Z, Wang J F, Huang Y M, Deng L, Xi T, Ma L, Hu T, Li L, Liu N L, Koidl F, Wang P, Chen Y A, Wang X B, Steindorfer M, Kirchner G, Lu C Y, Shu R, Ursin R, Scheidl T, Peng C Z, Wang J Y, Zeilinger A, and Pan J W 2018 *Phys. Rev. Lett.* **120** 030501

[29] Dynes J F, Wonfor A, Tam W W S, Sharpe A W, Takahashi R, Lucamarini M, Plews A, Yuan Z L, Dixon A R, Cho J, Tanizawa Y, Elbers J P, Greißer H, White I H, Penty R V, and Shields A J 2019 *npj Quantum Inf.* **5** 101

[30] Elliott C, Colvin A, Pearson D, Pikalo O, Schlafer J, and Yeh H 2005 *Current status of the DARPA quantum network Quantum Information and Computation III Quantum Information and Computation III* (SPIE) p. 138

[31] Peev M, Pacher C, Alléaume R, Barreiro C, Bouda J, Boxleitner W, Debuisschert T, Diamanti E, Dianati M, Dynes J F, Fasel S, Fossier S, Fürst M, Gautier J D, Gay O, Gisin N, Grangier P, Happe A, Hasani Y, Hentschel M, Hübel H, Humer G, Länger T, Legré M, Lieger R, Lodewyck J, Lorünser T, Lütkenhaus N, Marhold A, Matyus T, Maurhart O, Monat L, Nauerth S, Page J B, Poppe A, Querasser E, Ribordy G, Robyr S, Salvail L, Sharpe A W, Shields A J, Stucki D, Suda M, Tamas C, Themel T, Thew R T, Thoma Y, Treiber A, Trinkler P, Tualle-Brouri R, Vannel F, Walenta N, Weier H, Weinfurter H, Wimberger I, Yuan Z L, Zbinden H, and Zeilinger A 2009 *New J. Phys.* **11** 075001

[32] Sasaki M, Fujiwara M, Ishizuka H, Klaus W, Wakui K, Takeoka M, Miki S, Yamashita T, Wang Z, Tanaka A, Yoshino K, Nambu Y, Takahashi S, Tajima A, Tomita A, Domeki T, Hasegawa T, Sakai Y, Kobayashi H, Asai T, Shimizu K, Tokura T, Tsurumaru T, Matsui M, Honjo T, Tamaki K, Takesue H, Tokura Y, Dynes J F, Dixon A R, Sharpe A W, Yuan Z L, Shields A J, Uchikoga S, Legré M, Robyr S, Trinkler P, Monat L, Page J B, Ribordy G, Poppe A, Allacher A, Maurhart O, Länger T, Peev M, and Zeilinger A 2011 *Opt. Express* **19** 10387

[33] Yang Y H, Li P Y, Ma S Z, Qian X C, Zhang K Y, Wang L J, Zhang W L, Zhou F, Tang S B, Wang J Y, Yu Y, Zhang Q, and Pan J W 2021 *Opt. Express* **29** 25859

[34] Long G L and Liu X S 2002 *Phys. Rev. A* **65** 032302

[35] Pan D, Lin Z, Wu J, Zhang H, Sun Z, Ruan D, Yin L, and Long G L 2020 *Photon. Res.* **8** 1522

[36] Chen Y A, Zhang Q, Chen T Y, Cai W Q, Liao S K, Zhang J, Chen K, Yin J, Ren J G, Chen Z, Han S L, Yu Q, Liang K, Zhou F, Yuan X, Zhao M S, Wang T Y, Jiang X, Zhang L, Liu W Y, Li Y, Shen Q, Cao Y, Lu C Y, Shu R, Wang J Y, Li L, Liu N L, Xu F, Wang X B, Peng C Z, and Pan J W 2021 *Nature* **589** 214

[37] Bennett C H 1992 *Phys. Rev. Lett.* **68** 3121

[38] Muller A, Herzog T, Huttner B, Tittel W, Zbinden H, and Gisin N 1997 *Appl. Phys. Lett.* **70** 793

[39] Gisin N, Fasel S, Kraus B, Zbinden H, and Ribordy G 2006 *Phys. Rev. A* **73** 022320

[40] Mo X F, Zhu B, Han Z F, Gui Y Z, and Guo G C 2005 *Opt. Lett.* **30** 2632

[41] Chen T Y, Fang X T and Pan J W Patents No.201710365576.1

[42] Zhang G W, Ding Y Y, Chen W, Wang F X, Ye P, Huang G Z, Wang S, Yin Z Q, An J M, Guo G C, and Han Z F 2021 *Photonics Res.* **9** 2176

[43] Xu H, Wang S, Huang Y, Song Y, and Wang C 2020 *Appl. Sci.* **10** 1661

[44] Han Z F, Mo X F, Gui Y Z, and Guo G C 2005 *Appl. Phys. Lett.* **86** 221103